Bulletin of the Seismological Society of America, Vol. 97, No. 1A, pp. S223–S231, January 2007, doi: 10.1785/0120050627

Rupture Process of the 2004 Sumatra–Andaman Earthquake from Tsunami Waveform Inversion

by Alessio Piatanesi and Stefano Lorito

Abstract The aim of this work is to infer the slip distribution and rupture velocity along the rupture zone of the 26 December 2004 Sumatra–Andaman earthquake from available tide gage records of the tsunami. We selected waveforms from 14 stations, distributed along the coast of the Indian Ocean. Then we subdivided the fault plane into 16 subfaults (both along strike and downdip) following the geometry and mechanism proposed by Banerjee *et al.* (2005) and computed the corresponding Green's functions by numerical solution of the shallow-water equations through a finite-difference method. The slip distribution and rupture velocity were determined simultaneously by means of a simulated annealing technique. We compared the recorded and synthetic waveforms in the time domain, using a cost function that is a trade-off between the L1 and L2 norms. Preliminary tests on a synthetic dataset, together with *a posteriori* statistical analysis of the model ensemble enabled us to assess the effectiveness of the method and to quantify the model uncertainty. The main finding is that the best source model features a nonuniform distribution of coseismic slip, with high slip values concentrated into three main patches: the first is located in the southern part of the fault, off the coast of the Aceh Province; the second between 6.5° N and 11° N; and the third at depth, between 11° N and 14° N. Furthermore, we estimated that the rupture propagated at an average speed of 2.0 km/sec.

Introduction

On 26 December 2004, an earthquake of M_W 9.3 (Stein and Okal, 2005) struck the Sumatra–Andaman region and generated a huge tsunami. This was the most devastating and deadly event of this type that has occurred during the last centuries, causing more than 250,000 fatalities and spreading destruction along the coasts of the whole Indian Ocean.

Initially, the exceptional rupture extent and duration of the earthquake made it difficult to retrieve the details of the whole source mechanism using classical inversion methods. Actually, the problem of determining the rupture properties of this earthquake is still unresolved: several proposed source models, using different geophysical datasets (seismological, geodetic, hydroacoustic, etc.), differ in length, width, slip, and rupture velocity (e.g. Ammon *et al.*, 2005; Banerjee *et al.*, 2005; Bilham, 2005; de Groot-Hedlin, 2005; Fine *et al.*, 2005; Guilbert *et al.*, 2005; Ishii *et al.*, 2005; Krüger and Ohrnberger, 2005; Lay *et al.*, 2005; Park *et al.*, 2005; Stein and Okal, 2005; Tsai *et al.*, 2005; Vigny *et al.*, 2005).

Tsunami data can help resolve some of these source parameters. In fact, it has been shown that tide gage records and runup heights are useful to constrain some earthquake source parameters. In particular, they have good resolving power of the spatial extent and slip distribution for a tsunamigenic earthquake (e.g. Satake, 1987; Johnson *et al.*, 1996; Piatanesi *et al.*, 1996; Geist, 1999; Ortiz and Bilham, 2003). It has been also shown that near-field tsunami data may be used to retrieve information on the size and rheologic properties of a tsunamigenic slump or landslide (Heinrich *et al.*, 2001). This work deals with the problem of inferring the coseismic slip distribution for the 2004 Sumatra–Andaman earthquake using the available tide gage records of the tsunami. Furthermore, since the rupture duration of the Sumatra earthquake is exceptionally long, of the order of 10 min (e.g., Guilbert *et al.*, 2005; Ishii *et al.*, 2005; Krüger and Ohrnberger, 2005; Ni *et al.*, 2005; Park *et al.*, 2005; Stein and Okal, 2005; Tsai *et al.*, 2005), we will use the tsunami data also to infer the speed of rupture propagation. We first describe the method and the data selection and processing and then we discuss a synthetic test used to check the effectiveness of our technique. Finally we show the results obtained for the Sumatra earthquake and tsunami.

Forward Modeling and Green's Functions

Tsunamis are considered long shallow-water gravity waves, since their wavelength is usually much larger than

the sea depth. In this study we use the nonlinear shallow-water equations written as follow:

$$\begin{cases} \dfrac{\partial(z + h)}{\partial t} + \nabla \cdot [\mathbf{v}(z + h)] = 0 \\ \dfrac{\partial \mathbf{v}}{\partial t} + (\mathbf{v} \cdot \nabla)\mathbf{v} = -g\nabla z + \mathbf{C} + \mathbf{F}. \end{cases} \quad (1)$$

In equation (1), z represents the water elevation above sea level, h the water depth in a still ocean, $\mathbf{v}$ the depth-averaged horizontal velocity vector, and g the gravity acceleration; $\mathbf{C}$ and $\mathbf{F}$ represent the Coriolis and bottom friction forces, respectively. The boundary conditions are pure wave reflection at the solid boundary (coastlines) and full wave transmission at the open boundary (open sea). The equations are solved numerically by means of a finite-difference method on a staggered grid. The initial seawater elevation is assumed to be equal to the coseismic vertical displacement of the sea bottom, computed through the Okada's analytical formulas (Okada, 1992), while the initial velocity field is assumed to be identically zero. Numerical modeling of the tsunami is carried out in the domain depicted in Figure 1 with 1 arc-minute of spatial resolution, using the ETOPO2 bathymetric dataset (Smith and Sandwell, 1997). This dataset is supposed to be inaccurate in very shallow waters and it may constitute an additional source of error. A good practice is that followed by Fujii and Satake (2007) and by Geist *et al.* (2006), which merged different bathymetric datasets.

The usual way to deal with the problem of retrieving the slip distribution on the fault from tsunami data is to first subdivide the fault plane into a number of subfaults and compute the Green's function (i.e., the tsunami waveform at a station produced by a subfault) by solving the linear form of equation (1). The tsunami waveforms produced by the whole source are then calculated as a linear combination of the Green's functions corresponding to each subfault, multiplied by a coefficient that is the actual slip amount. It is evident that this method holds if the linear equations are valid for propagation of the entire wave field. For tsunami propagation in very shallow water and when the wave amplitude is large, the linear approximation is no longer valid. We find that this is what happens in some regions (for instance, along the coast of Thailand), characterized by a very large and very shallow continental shelf and when the incoming tsunami wave exceeds a few meters of amplitude. Using the nonlinear equation (1), we compute two waveforms corresponding to a subfault with 1 and 10 m of slip, respectively, and find that the two waveforms do not scale by a simple factor 10, as expected if propagation were linear. Without abandoning the idea that the whole source may be viewed as a combination of elementary sources, we follow a nonconventional approach to compute the Green's functions for our problem: instead of solving the linear equations and assuming unitary slip amplitude on a subfault, we use the nonlinear shallow-water equations and 10 m of slip amplitude for each elementary subfault. We use 10 m of slip for the elementary source, since this is the mean slip along the whole fault compatible with seismic moment estimations (Stein and Okal, 2005). It is reasonable to assume that the slip value for each subfault of heterogeneous source will be centered on this mean value. From this point of view, our approach to compute the Green's functions may be seen as a way to linearize the problem around the mean slip value.

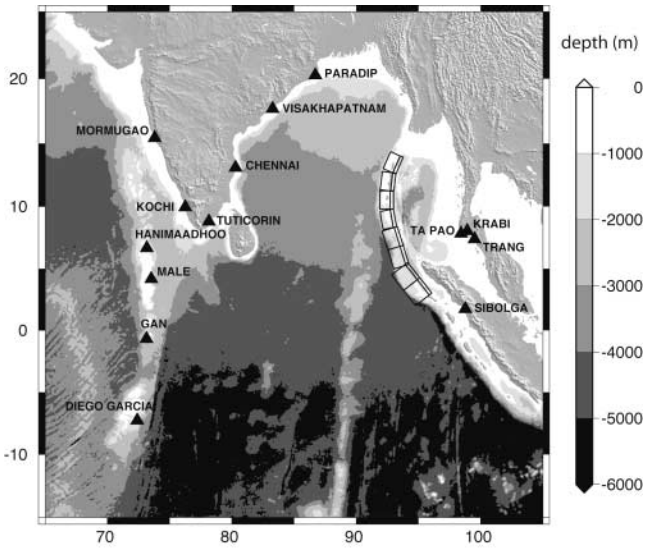

Figure 1. Map of the computational domain and location of the tide gages and boundaries of the subfaults (surface projection) used in this work.

Waveform Selection and Processing

The 26 December 2004 Sumatra–Andaman tsunami propagated worldwide and was recorded by several tide gages in the Indian Ocean, as well as by stations in both the Pacific and Atlantic Oceans (Merrifield *et al.*, 2005; Nagarajan *et al.*, 2006; Tanioka *et al.*, 2006; Tsuji *et al.*, 2006).

After careful inspection of the available records, we select 14 stations that are azimuthally distributed along the coast of the Indian Ocean (see Fig. 1). Some of these records have been manually digitized at a sampling interval of 5 min while others were recorded by digital instruments, with sampling intervals ranging from 2 to 10 min (see Table 1 for a summary). We choose a time window that includes only the first oscillations in the waveforms, since errors in the bathymetric dataset and the coarse grid does not allow modeling of local effects (e.g., resonance of the bays) that may contribute to later arrivals (coda) on the recorded waveforms.

Global Search Inverse Technique

The observed and synthetic waveforms are compared in the time domain. A key issue in inverse problems is choosing

Table 1
List of Tide Gage Stations

Station	Latitude	Longitude	Analog/ Digital	Sampling Interval (min)	Relative Weight for Sampling Interval	Relative Weight for Azimuthal Distribution
Krabi	08.05° N	98.92° E	A	5	0.75	0.67
Trang	07.40° N	99.52° E	A	5	0.75	0.67
Ta pao	07.77° N	98.42° E	A	5	0.75	0.67
Sibolga	01.75° N	98.77° E	D	10	0.5	1
Diego Garcia	07.28° S	72.40° E	D	6	0.75	1
Gan	00.68° S	73.15° E	D	4	1	1
Male	04.18° N	73.52° E	D	4	1	1
Hanimaadhoo	06.67° N	73.17° E	D	2	1	1
Visakhapatnam	17.68° N	83.28° E	D	5	0.75	1
Paradip	20.26° N	86.70° E	D	6	0.75	1
Chennai	13.10° N	80.30° E	D	5	0.75	1
Tuticorin	08.80° N	78.15° E	D	6	0.75	1
Kochi	09.96° N	76.26° E	D	6	0.75	1
Mormugao	15.42° N	73.80° E	D	5	0.75	1

a suitable cost function to represent the goodness of fit for a given model. A widely used approach is to minimize the L_2 norm, since this leads to easy computations taking the form of a least-squares problem. The main drawback is that the least-squares solutions are not robust. In fact, they are very sensitive to a small number of large errors in the dataset (Tarantola, 1987). Here we use an objective function that is a hybrid representation between L_1 and L_2 norm (Sen and Stoffa, 1991) that can be written as

$$E(\mathbf{m}) = \sum_{k=1}^{N} \left[1 - \frac{2\sum_{t_i}^{t_f} (u_0(t)u_S(t))}{\sum_{t_i}^{t_f} u_0^2(t) + \sum_{t_i}^{t_f} u_S^2(t)} \right]_k . \quad (2)$$

In equation (2) u_0 and u_S are the observed and synthetic waveforms, respectively; t_i and t_f are the lower and upper bounds of the time window; and N is the number of records used in the inversion. This cost function takes information from both the shape and the amplitude of a waveform and is more robust than the standard least-squares technique.

The general forward problem may be written as

$$\mathbf{d} = \mathbf{G}(\mathbf{m}). \quad (3)$$

Here **d** represents the theoretical data values (tsunami waveforms), **m** are the parameters describing the model (slip amplitude and rupture velocity), and **G** is a function linking the observables to the model. The problem of inverting tsunami waveforms to determine slip distribution on the fault was originally formulated by Satake (1987) as a linear inverse problem. In this case **G**, the Green's functions, do not depend on **m** and the problem may be solved using a generalized inverse of **G**. The Green's functions used to assemble the matrix **G** should depend on the rupture velocity as they have to account for the appropriate time delay of the unit sources. In Satake's (1987) work the unit sources turn on at the same time, thus implicitly assuming an infinite rupture velocity along the whole fault. In this work we invert for both the slip distribution and the rupture velocity simultaneously. In this case, **G** will depend on the rupture velocity, which is one of the parameters to be inverted, thus leading to a nonlinear inverse problem.

To deal with this problem, we use a global optimization method that is a particular implementation of the simulated annealing technique, called the "heat bath algorithm" (Rothman, 1986). This technique, already used in nonlinear finite-fault inversion (e.g., Ji *et al.*, 2002; Liu and Archuleta, 2004), performs a large sampling of the model space and concentrates the search on regions characterized by low values of the cost function, that is, where the optimal models are likely to be found.

Synthetic Test

To check the effectiveness of our method in inverting for both the slip distribution and the rupture velocity, we perform a synthetic checkerboard test. We subdivide the fault plane into 16 subfaults, following the geometry and mechanism proposed by Banerjee *et al.* (2005) from analysis of far-field static displacements recorded by Global Positioning System (GPS) measurements. The parameters characterizing each subfault are listed in Table 2. Then we build a test rupture model that consists of a slip distribution having a checkerboard pattern, with slip values alternating between 5 and 15 m. The velocity of the rupture front is taken at 2 km/sec. The synthetic waveforms are then resampled at the same intervals as the observed data (see Table 1) and corrupted by adding a Gaussian random noise with a variance that is 10% of the clean waveform amplitude variance (Ji *et al.*, 2002). The artificial noise level we introduce is at least three times larger than the background noise of the tide

Table 2
Subfault Parameters

Fault Segment	Longitude* E	Latitude* N	Width (km)	Length (km)	Strike (°)	Rake (°)	Dip (°)	Top (km)	Bottom (km)	Slip (m) Best	Slip (m) Average
1 Deep	96.073	3.028	35	175	322	90	35	30	50	10	13.4
1 Shallow	95.868	2.870	157	175	322	90	11	0	30	11	12.8
2 Deep	95.103	4.268	35	175	322	90	35	30	50	30	21.4
2 Shallow	94.898	4.110	157	175	322	90	11	0	30	10	11.2
3 Deep	94.233	5.352	35	178	343	105	35	30	50	6	12.6
3 Shallow	93.982	5.277	116	178	343	105	15	0	30	0	6.2
4 Deep	93.764	6.879	35	178	343	105	35	30	50	8	11.7
4 Shallow	93.511	6.803	116	178	343	105	15	0	30	11	12.7
5 Deep	93.238	8.355	35	163	350	105	35	30	50	8	12.8
5 Shallow	92.975	8.311	97	163	350	105	18	0	30	13	14.9
6 Deep	92.987	9.799	35	163	0	115	35	30	50	4	12.5
6 Shallow	92.716	9.799	97	163	0	115	18	0	30	11	15
7 Deep	93.015	11.198	35	163	7	122	35	30	50	13	14.3
7 Shallow	92.741	11.229	97	163	7	122	18	0	30	6	9.7
8 Deep	93.182	12.570	35	163	24	139	35	30	50	26	17.5
8 Shallow	92.925	12.675	97	163	24	139	18	0	30	0	8.9

*Longitude and latitude refer to the southernmost point on lower edge of each subfault.

gage records before the first tsunami arrival. We assign a relative weight to each station in order to take into account nonuniformity in both the sampling rate of the records and azimuthal distribution of the stations (see Table 1). We introduce *a priori* information on the model solution by imposing lower and upper bounds to the range of possible source parameters, namely 0–30 m for the slip amplitude and 0.25–5.0 km/sec for the rupture velocity.

The best inverted model is very similar to the target one: the checkerboard shape of the slip distribution is well reproduced and the rupture velocity is estimated exactly (see Figs. 2 and 3). The test and inverted models are not strictly identical in terms of slip for some subfaults, especially for those located in the northern part of the rupture zone. Nevertheless, because the cost function of the inverted model is very low and the comparison of the observed and synthetic waveforms is good (Fig. 4), it is likely that the problem is ill conditioned and the solution is not unique.

Simple Appraisal of the Ensemble

During the search stage of the simulated annealing method, a large number of models are tested (about 1 million) and the corresponding cost function computed. All of these models represent a sample of the model space that may be viewed as a statistical ensemble. An important step of a nonlinear inverse method is the appraisal stage, where some information of the model solution is inferred from the whole ensemble (e.g., Mosegaard and Tarantola, 1995; Sambridge and Mosegaard, 2002). Other interesting properties may be extracted from the ensemble, such as the mean and the variance. Figure 2 shows the marginal distribution corresponding to each parameter, together with the values of the best model. To emphasize the properties of those models that are most suitable (i.e., with small value of the cost function E),

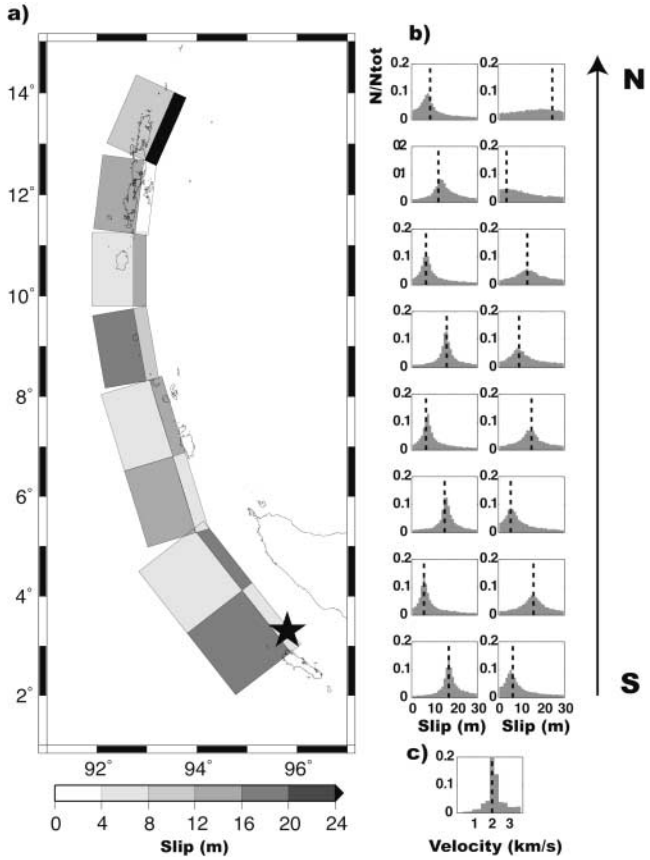

Figure 2. (a) Slip distribution of the best model resulting from the checkerboard test: the rectangles represent the projection of the subfaults to the Earth's surface. (b) Marginal distributions of the slip amplitude corresponding to each subfault: shallow subfaults in the left-hand column; deep subfaults in the right-hand column. (c) Marginal distribution for the rupture velocity. In (b) and (c) vertical dashed lines represent the best model values of each parameter.

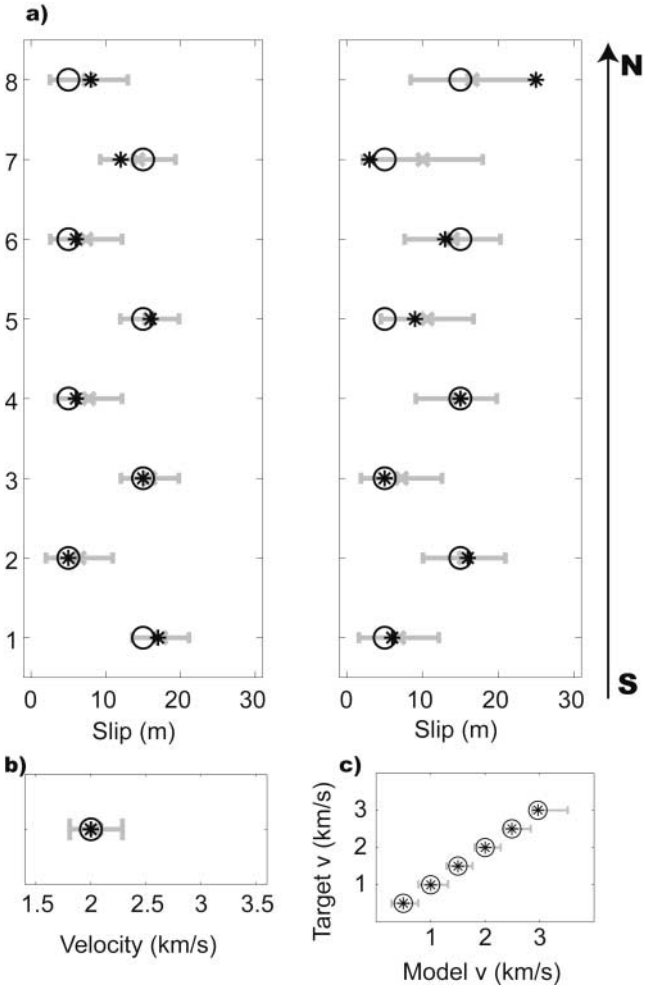

Figure 3. (a) Standard deviation ($\pm\sigma$ interval, gray line), average (gray cross), best (black star) and target (black circle) slip amplitude (in meters) for the synthetic checkerboard test: shallow subfaults in the left-hand column, deep subfaults in the right-hand column. (b) Same as (a) for rupture velocity (in km/sec). (c) same as (a), with target velocities ranging from 0.5 to 3.5 km/sec, at 0.5 km/sec steps.

we calculate a weighted mean and standard deviation of each parameter, using as weighting function $w = 1/E$ (Shibutani *et al.*, 1996). The standard deviation may be interpreted as the uncertainty in the estimation of the corresponding parameter. Smaller values of the standard deviation indicate that the corresponding parameters are better resolved than those characterized by larger deviations. In general, the distributions are strongly peaked around the mean and both the best and the target models are always found within 1 standard deviation of the mean (see Fig. 3). Nevertheless, the standard deviations increase from south to north: this can be interpreted as a decrease in the resolution for parameters in the northernmost subfaults. To a smaller extent, it appears that the shallow subfaults are better resolved than the deep ones. Surprisingly, one of the best resolved parameter is the mean rupture velocity, for which the corresponding marginal distribution features a well-defined peak, centered on the value of the target model. We furthermore examine the sensitivity of the tsunami waveforms to variation in rupture velocity. We perform synthetic tests with different target rupture velocities, ranging from 0.5 km/sec to 3.0 km/sec at 0.5 km/sec intervals. Figure 3c clearly shows that the best model in all cases exactly estimates the mean rupture velocity. Moreover, the standard deviation tends to slightly increase with the velocity value of the target model. At least for this exceptionally long earthquake, the tide-gage records are able to constrain the mean rupture speed.

Application to the 2004 Sumatra Earthquake

The results of the synthetic test are encouraging: they show that the nonlinear inversion method and the station distribution are able to resolve the rupture process, thus allowing us to apply this procedure to the 2004 Sumatra tide gage data.

The results of the inversion are summarized in Figure 5, where we show the slip distribution corresponding to the best model found during the whole search of the parameter space. The slip distribution is strongly heterogeneous, with high slip concentrated in three main patches. The first is located in the southern part of the fault and extends from the hypocenter to about 5° N: the mean slip exceeds 10 m with a high concentration of 30 m on the deep subfault just off the Aceh Province. This region of high slip is consistent with the severe inundation and runup observed along the coast of the Aceh Province and in Banda Aceh, reaching 30 m in some places. The second main region of slip is located between 6.5° N and 11° N, with a mean slip of about 10 m, mainly distributed on the shallow part of the fault. A third concentration of slip appears in the northernmost deep part of the fault with a mean slip of about 20 m. The mean speed of the rupture is estimated to be 2.0 km/sec. We performed *a posteriori* analysis on the model ensemble to assess the uncertainty and the resolution of the model solution, in the same way as described above for the synthetic test. In Figure 5, we show the marginal distribution corresponding to each parameter, together with the values of the best model. The marginal distributions relative to most subfaults feature a distinct peak, thus indicating a fairly good resolution of the corresponding parameter. As expected from what we learned with the synthetic test, there is a loss of resolution from south to north and, in general, the shallow segments are better resolved than the deeper ones. In particular the high slip value we find in the northernmost part of the fault at depth is poorly resolved and probably overestimated, as revealed by the results of the synthetic checkerboard test. Furthermore, differently from what found in the synthetic test, the values corresponding to the best model are often at the edge of one standard deviation interval: this reveals that the real records are affected by other sources of error than the noise injected into the synthetics. In general, when the marginal are large the output should be interpreted with great

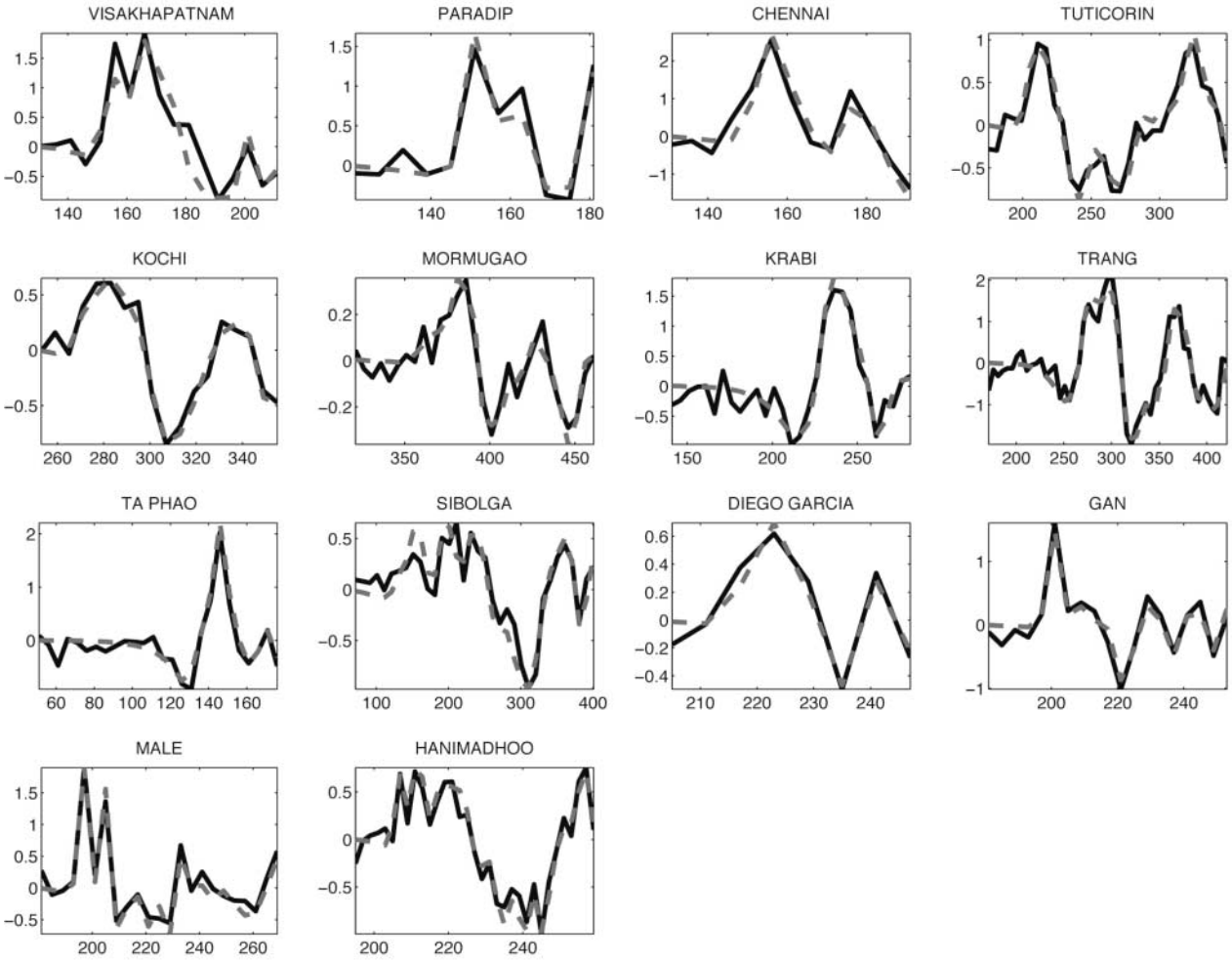

Figure 4. Comparison between the waveforms corresponding to the target (black solid) and the inverted best model (gray dashed) for the checkerboard test. Amplitudes are in meters and time window in minutes after the earthquake origin time.

care (Mosegaard and Sambridge, 2002): in such cases the best model should be regarded as an outlier (see Fig. 6). The comparison of the recorded and synthetic waveforms generally shows a good agreement (Fig. 7). Nevertheless, some tide gages do not show some of the high-frequency content in the synthetic waveforms. This may be due to the sampling interval of the records and most probably to a poor instrumental response of the tide gages, which are generally designed to measure ocean tides at periods much longer than tsunami waves.

Conclusions

Our method makes use of tsunami waveforms, recorded by several tide gages in the Indian Ocean to infer the finite-fault rupture process of the 2004 Sumatra earthquake. To our knowledge, this is the first time that a nonlinear inversion method (simulated annealing technique) is applied to tsunami data to retrieve simultaneously the slip distribution and the rupture velocity. We find a heterogeneous distribution of the slip, characterized by three distinct patches: the first is located in the southern part of the fault, off the coast of the Aceh Province; the second between 6.5° N and 11° N; and the third at depth, between 11° N and 14° N. This is in fairly good agreement with the model proposed by Subarya *et al.* (2006), derived from inverting near-field GPS surveys in northern Sumatra and observations of the vertical motion of coral reefs: they found three main patches, with the highest slip offshore of Banda Aceh and a significant amount of slip at depth in the northernmost end. We also find reasonable agreement in both slip amplitude and distribution with model C of Ammon *et al.* (2005), derived from teleseismic body waves (5–200 sec), intermediate-period regional seismograms (50–500 sec) and long-period teleseismic seismograms (250–2000 sec). These authors found a large slip release between 3° N and 6° N and, to a smaller extent, up to 10° N. As they noted, larger amounts of slip are needed north of 8° N to explain GPS displacements in the Nicobar and Andaman Islands: the second patch of our model (see Fig. 5) extends from 6.5° N to 11° N and has 10 m of mean slip,

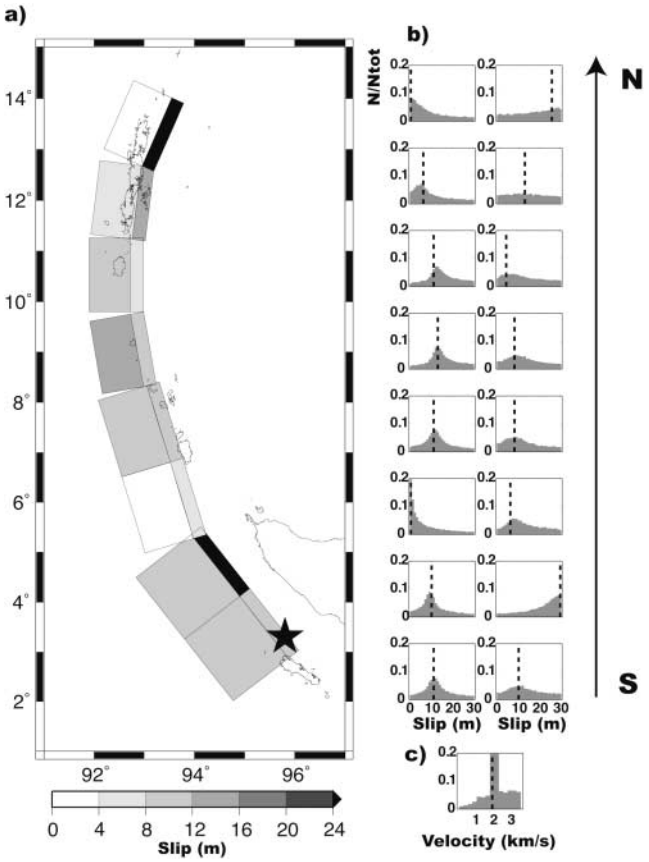

Figure 5. (a) Slip distribution of the best model for the Sumatra earthquake: the rectangles represent the projection of the subfaults to the Earth's surface. (b) Marginal distributions of the slip amplitude corresponding to each subfault: shallow subfaults in the left-hand column, deep subfaults in the right-hand column. (c) Marginal distribution for the rupture velocity. Vertical dashed lines represent the best model.

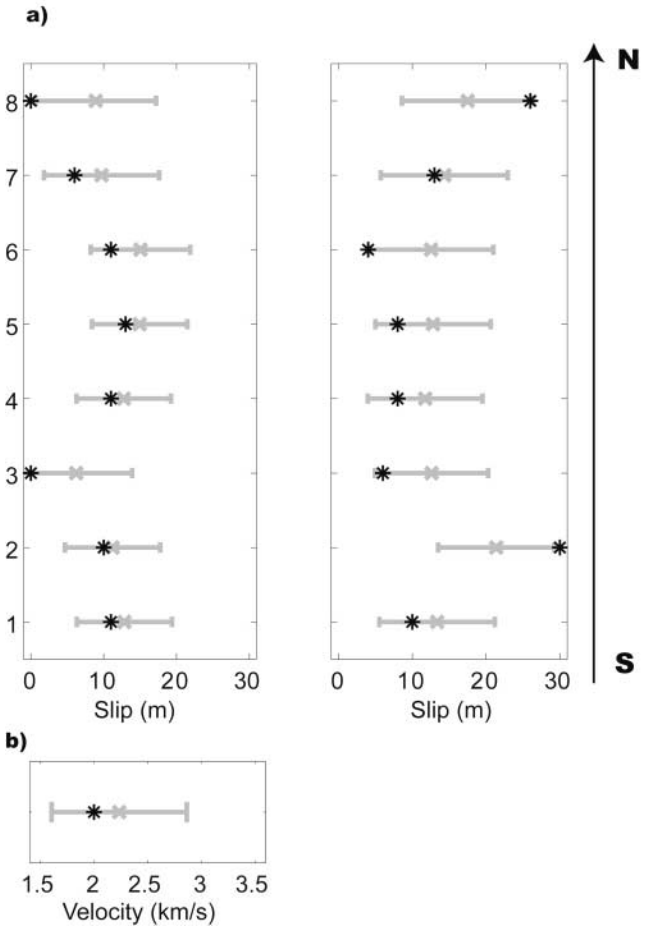

Figure 6. (a) Standard deviation ($\pm\sigma$ interval, gray line), average (gray cross), best (black star) slip amplitude (in meters) corresponding to the inverted model for the Sumatra earthquake: shallow subfaults in the left-hand column, deep subfaults in the right-hand column. (b) Same as (a) for the rupture velocity (in km/sec).

slightly larger than Ammon's *et al.* (2005) model, and could be consistent with geodetic observations.

Though we are using a different parametrization of the source, we find a partial agreement with other authors who invert tsunami data to reconstruct the source process. In particular our results are roughly consistent with those obtained by Tanioka *et al.* (2006) from tide gage records and coseismic vertical deformation observed along the coast: they find large slip off Banda Aceh and a relevant slip release between 7° N and 11° N. Conversely, their results do not show any relevant slip north of 12° N: to this respect the model obtained from satellite altimetry by Hirata *et al.* (2006) is more consistent with our findings.

Assuming a rigidity $\mu = 3.0 \times 10^{10}$ N/m^2, the seismic moment of our best model is $M_0 = 5.7 \times 10^{22}$ N m, corresponding to $M_w = 9.1$, whereas that of the mean model is $M_0 = 7.5 \times 10^{22}$ N m, corresponding to $M_w = 9.2$. These values agree with other estimates based on seismological data. Our nonlinear inverse method enables us to also estimate a mean rupture velocity of about 2.0–2.25 km/sec. This is consistent with some seismological results (e.g., Ammon *et al.* [2005] $v = 2.5$ km/sec; Kruger and Ohrnberger [2005] $v = 2.3$–2.7 km/sec) and those obtained by inversion of tide gage records by Tanioka *et al.* (2006) ($v = 1.7$ km/sec). Conversely, our estimate of the rupture speed differs from those of Ishii *et al.* (2005) ($v = 2.8$ km/sec, from seismological data), Fujii and Satake (2006) ($v = 1.0$ km/sec, from joint inversion of tide gage and satellite altimetry), and Hirata *et al.* (2006) ($v = 0.7$ km/sec, from satellite altimetry).

Some authors suggested that the slip in the northern section of the rupture zone may have been released very slowly, at a timescale beyond the seismic band (Bilham, 2005). The model parameterization we adopt in this work enables us to estimate only the mean rupture speed. This aspect of the source process as well as a refinement of the source geometry (e.g., Banerjee *et al.*, 2007; Subarya *et al.*, 2006) may be the subject for future investigations.

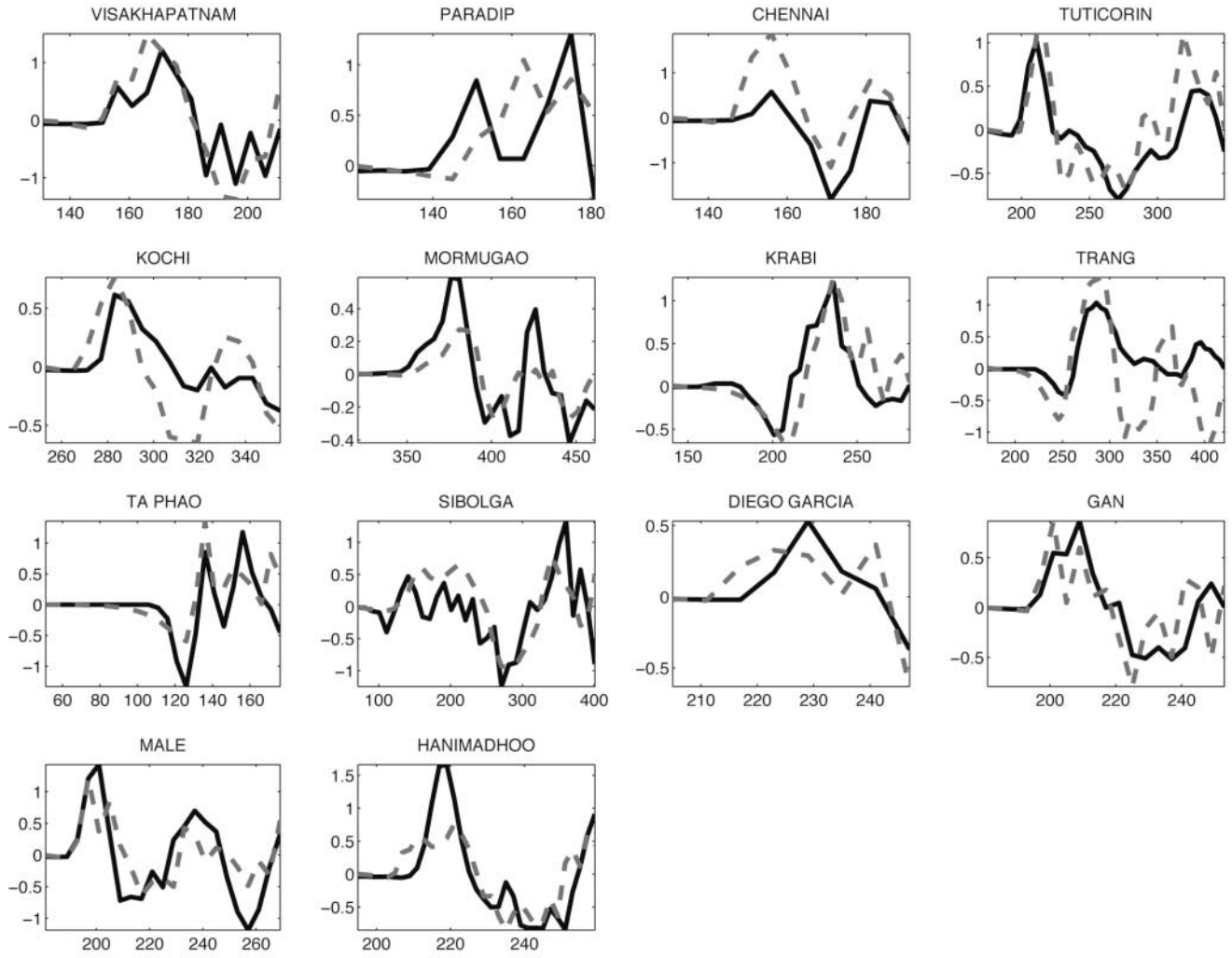

Figure 7. Comparison between the tide gage records (black solid) and the waveforms computed using the inverted best model (gray dashed). Amplitudes are in meters and time window in minutes after the earthquake origin time.

Acknowledgments

Comments from K. Satake, E. Geist, and an anonymous reviewer greatly improved the manuscript. Some figures have been produced with Generic Mapping Tools (Wessel and Smith, 1998).

References

Ammon, C. J., C. Ji, H. K. Thio, D. Robinson, S. Ni, V. Hjorleifsdottir, H. Kanamori, T. Lay, S. Das, D. Helmberger, G. Ichinose, J. Polet, and D. Wald (2005). Rupture process of the 2004 Sumatra–Andaman earthquake, *Science* **308,** 1133–1139.

Banerjee, P., F. F. Pollitz, and R. Bürgmann (2005). The size and duration of the Sumatra–Andaman earthquake from far-field static offsets, *Science* **308,** 1769–1772.

Banerjee, P., F. F. Pollitz, B. Nagarajan, and R. Bürgmann (2007). Coseismic slip distributions of the 26 December 2004 Sumatra–Andaman and 28 March 2005 Nias earthquakes from Global Positioning System (GPS) static offsets, *Bull. Seism. Soc. Am.* **97,** no. 1A, S86–S102.

Bilham, R. (2005). A flying start, then a slow slip, *Science* **308,** 1126–1127.

de Groot-Hedlin, C. D. (2005). Estimation of the rupture length and velocity of the Great Sumatra earthquake of Dec 26, 2004 using hydroacoustic signals, *Geophys. Res. Lett.* **32,** L11303, doi 10.1029/2005GL022695.

Fine, I. V., A. B. Rabinovich, and R. E. Thomson (2005). The dual source region for the 2004 Sumatra tsunami, *Geophys. Res. Lett.* **32,** L16602, doi 10.1029/2005GL023521.

Fujii, Y., and K. Satake (2007). Tsunami source of 2004 Sumatra–Andaman earthquake inferred from tide-gauges and satellite data, *Bull. Seism. Soc. Am.* **97,** no. 1A, S192–S207.

Geist, E. (1999). Local tsunamis and earthquake source parameters, *Adv. Geophys.* **39,** 117–209.

Geist, E., V. V. Titov, D. Arcas, F. P. Pollitz, and S. L. Bilek (2007). Implications of the 26 December 2004 Sumatra–Andaman earthquake on tsunami forecast and assessment models for great subduction zone earthquakes, *Bull. Seism. Soc. Am.* **97,** no. 1A, S249–S270.

Guilbert, J., J. Vergoz, E. Scisselé, A. Roueff, and Y. Cansi (2005). Use of hydroacoustic and seismic arrays to observe rupture propagation and source extent of the $M_W = 9.0$ Sumatra earthquake, *Geophys. Res. Lett.* **32,** L15310, doi 10.1029/2005GL022966.

Heinrich, P., A. Piatanesi, and H. Hebert (2001). Numerical modelling of tsunami generation and propagation from submarine slumps: the 1998 Papua New Guinea event, *Geophys. J. Int.* **145,** 97–111.

Hirata, K., K. Satake, Y. Tanioka, T. Kuragano, Y. Hasegawa, Y. Hayashi, and N. Hamada (2006). The 2004 Indian ocean tsunami: tsunami source model from satellite altimetry, *Earth Planets Space* **58,** 195–201.

Ishii, M., P. M. Shearer, H. Houston, and J. Vidale (2005). Extent, duration and speed of the 2004 Sumatra–Andaman earthquake imaged by the Hi-Net array, *Nature* **435,** 933–936.

Ji, C., D. J. Wald, and D. V. Helmberger (2002). Source description of the 1999 Hector Mine, California earthquake, part I: Wavelet domain inversion theory and resolution analysis, *Bull. Seism. Soc. Am.* **92,** no. 4, 1192–1207.

Johnson, J. M., K. Satake, S. R. Holdahl, and J. Sauber (1996). The 1964 Prince Williams Sound Earthquake: joint inversion of tsunami and geodetic data, *J. Geophys. Res.* **101,** 523–532.

Krüger, F., and M. Ohrnberger (2005). Tracking the rupture of the M_W = 9.3 Sumatra earthquake over 1,150 km at teleseismic distance, *Nature* **435,** 937–939.

Lay, T., H. Kanamori, C. J. Ammon, M. Nettles, S. N. Ward, R. C. Aster, S. L. Beck, S. L. Bilek, M. R. Brudzinski, R. Butler, H. R. De Shon, G. Ekström, K. Satake, and S. Sipkin (2005). The great Sumatra–Andaman earthquake of 26 December 2004, *Science* **308,** 1127–1133.

Liu, P., and R. J. Archuleta (2004). A new nonlinear finite fault inversion with three-dimensional Green's functions: application to the 1989 Loma Prieta, California, earthquake, *J. Geophys. Res.* **109,** B02318, doi 10.1029/2003JB002625.

Merrifield, M. A., Y. L. Firing, T. Aarup, W. Agricole, G. Brundritt, D. Chang-Seng, R. Farre, B. Kilonsky, W. Knight, L. Kong, C. Magori, P. Manurung, C. McCreery, W. Mitchell, S. Pillay, F. Schindele, F. Shillington, L. Testut, E. M. S. Wijeratne, P. Caldwell, J. Jardin, S. Nakahara, F.-Y. Porter, and N. Turetsky (2005). Tide gauge observations of the Indian Ocean tsunami, December 26, 2004, *Geophys. Res. Lett.* **32,** L09603, doi 10.1029/2005GL022610.

Mosegaard, K., and M. Sambridge (2002). Monte Carlo analysis of inverse problems, *Inverse Problems* **18,** R29–R54.

Mosegaard, K., and A. Tarantola (1995). Monte Carlo sampling of solutions to inverse problems, *J. Geophys. Res.* **100,** no. B7, 12,431–12,447.

Nagarajan, B., I. Suresh, D. Sundar, R. Sharma, A. K. Lal, S. Neetu, S. S. C. Shenoi, S. R. Shetye, and D. Shankar (2006). The great tsunami of 26 December 2004: a description based on tide-gauge data from the Indian subcontinent and surrounding areas, *Earth Planet Space* **58,** 211–215.

Ni, S., H. Kanamori, and D. Helmberger (2005). Energy radiation from the Sumatra earthquake, *Nature* **434,** 582.

Okada, Y. (1992). Internal deformation due to shear and tensile faults in a half-space, *Bull. Seism. Soc. Am.* **82,** 1018–1040.

Ortiz, M., and R. Bilham (2003). Source area and rupture parameters of the 31 December 1881 M_W = 7.9 Car Nicobar earthquake estimated from tsunamis recorded in the ay of Bengal, *J. Geophys. Res.* **108,** no. 4, doi 10.1029/2002JB001941.

Park, J., T. R. A. Song, J. Tromp, E. Okal, S. Stein, G. Roult, E. Clevede, G. Laske, H. Kanamori, P. Davis, J. Berger, C. Braitenberg, M. Van Camp, X. Lei, H. Sung, H. Xu, and S. Rosat (2005). Earth's free oscillations excited by the 26 December 2004 Sumatra–Andaman earthquake, *Science* **308,** 1139–1144.

Piatanesi, A., S. Tinti, and I. Gavagni (1996). The slip distribution of the 1992 Nicaragua earthquake from tsunami run-up data, *Geophys. Res. Lett.* **23,** no. 1, 37–40.

Rothman, D. (1986). Automatic estimation of large residual statics corrections, *Geophysics* **51,** 332–346.

Sambridge, M., and K. Mosegaard (2002). Monte Carlo methods in geophysical inverse problems, *Rev. Geophys.* **40,** no. 3, doi 10.1029/2000RG000089.

Satake, K. (1987). Inversion of tsunami waveforms for the estimation of a fault heterogeneity: method and numerical experiments, *J. Phys. Earth* **35,** 241–254.

Sen, M., and P. L. Stoffa (1991). Nonlinear one-dimensional seismic waveform inversion using simulated annealing, *Geophysics* **56,** 1624–1638.

Shibutani, T., M. Sambridge, and B. Kennett (1996). Genetic algorithm inversion for receiver functions with applications to crust and uppermost mantle structure beneath Eastern Australia, *Geophy. Res. Lett.* **23,** 1829–1832.

Smith, W. H. F., and D. T. Sandwell (1997). Global sea floor topography from satellite altimetry and ship depth soundings, *Science* **277,** 1956–1962.

Stein, S., and E. A. Okal (2005). Speed and size of the Sumatra earthquake, *Nature* **434,** 581–582.

Subarya, C., M. Chlieh, L. Prawirodirdjo, J-P. Avouac, Y. Boch, K. Sieh, A. J. Meltzmer, D. H. Natawidjaja, and R. McCaffrey (2006). Plate deformation associated with the great Sumatra–Andaman earthquake, *Nature* **440,** 46–51.

Tanioka, Y., Yudhicara, T. Kususose, S. Kathiroli, Y. Nishimura, S. I. Iwasaki, and K. Satake (2006). Rupture process of the 2004 great Sumatra–Andaman earthquake estimated from tsunami waveforms, *Earth Planet Space* **58,** 203–209.

Tarantola, A. (1987). *Inverse Problem Theory*, Elsevier Science, New York.

Tsai, V. C., M. Nettles, G. Ekström, and A. Dziewonski (2005). Multiple CMT source analysis of the 2004 Sumatra earthquake, *Geophys. Res. Lett.* **32,** L17304, doi 10.1029/2005GL023813.

Tsuji, Y., Y. Namegaya, H. Matsumoto, S.-I. Iwasaki, W. Kambua, M. Sriwichai, and V. Meesuk (2006). The 2004 Indian tsunami in Thailand: tsunami height and tide-gauge records, *Earth Planet Space* **58,** 223–232.

Vigny, C., W. J. F. Simons, S. Abu, R. Bamphenyu, C. Satirapod, N. Choosakul, C. Subaraya, A. Soquet, K. Omar, H. Z. Abidin, and B. A. C. Ambrosius (2005). Insight into the 2004 Sumatra–Andaman earthquake from GPS measurements in Southeast Asia, *Nature* **436,** 201–206.

Wessel, P., and W. H. F. Smith (1998). New, improved version of the Generic Mapping Tools released, *EOS Trans. AGU* **79,** 579.

Istituto Nazionale di Geofisica e Vulcanologia
Department of Seismology and Tectonophysics
Via di Vigna Murata 605, 00143 Rome, Italy
piatanesi@ingv.it
lorito@ingv.it

Manuscript received 24 January 2006.